Light Metals 2015
Edited by: Margaret Hyland
TMS (The Minerals, Metals & Materials Society), 2015

Light Metals 2015

ALUMINUM ALLOYS: DEVELOPMENT, CHARACTERIZATION AND APPLICATIONS

Advanced Analysis

SESSION CHAIR
Gang Sha
Nanjing University of
Science and Technology
Nanjing, China

Light Metals 2015
Edited by: Margaret Hyland
TMS (The Minerals, Metals & Materials Society), 2015

HYDROGEN VISUALIZATION IN THE DEFORMED MICROSTRUCTURE OF Al-Zn-Mg BASE ALLOYS

Keitaro Horikawa[1], Kenichi Tanigaki and Hidetoshi Kobayashi[1]
[1]Osaka University; 1-3 Machikaneyama Toyonaka, Osaka, 5608531, Japan

Keywords: Hydrogen, Visualization, Surface, Deformation, Inclusion

Abstract

Al-Zn-Mg base alloys prone to show hydrogen embrittlement (HE) when exposed and deformed under hydrogen related atmosphere. To suppress HE of the Al-Zn-Mg base alloys, the addition of copper is reported to be effective. However, the role of copper on the suppression of HE has not been fully cleared. In the present study, hydrogen in the deformed microstructure was visualized by means of hydrogen microprint technique together with mass spectrometry. Using HMT, it was revealed that hydrogen was released preferentially from grain boundaries, slip lines, and intermetallic particles. The tendency of hydrogen trapping around the particles was prominent in the Al-Zn-Mg alloys containing copper. In contrast, hydrogen was released mainly from localized slip lines and grain boundaries in the Al-Zn-Mg alloy without copper. The difference of hydrogen trapping state in the microstructure could be related to HE sensitivity of Al-Zn-Mg base alloys.

Introduction

Aluminum alloys have been regarded as one of the candidate liner materials for a high-pressure hydrogen tank in the fuel cell vehicles (FCVs), since aluminum alloys show high resistance to hydrogen embrittlement rather than the steels and other structural materials [1,2]. Among the commercial alloys, Al-Mg-Si base alloys are believed to be the most promising materials for the metallic tank liner [3]. It is also known that high strength aluminum alloys such as Al-Zn-Mg base (7000 series) one are susceptible to hydrogen embrittlemt when exposed to hydrogen environment [4-7]. Application of the high strength aluminium alloys has a benefit for the reduction of the weight of hydrogen tank liner materials. It is reported that the addition of Cu to an Al-Zn-Mg alloy is effective to reduce the sensitivity of hydrogen embrittlement [8]. However, detailed mechanism of the suppression of hydrogen embrittlement caused by the additional copper is not fully cleared of the Al-Zn-Mg base alloys. We assumed that detecting hydrogen gas evolution during deformation and fracture would be helpful to understand the mechanism of hydrogen embrittlement of Al-Zn-Mg base alloys. In the present study, hydrogen gas evolution in the tensile test of Al-Zn-Mg (-Cu) alloys was detected by using the experimental methods such as a hydrogen microprint technique (HMT) and a mass spectrometry.

Experimental

Al-Zn-Mg alloy (Alloy A) and Al-Zn-Mg-Cu alloy (Alloy B) were used in the present study; its chemical composition is shown in Table 1. After the homogenization at 450 ˚C for 15 h, the alloy ingots with a thickness of 70 mm were hot-rolled (410 ˚C) and cold-rolled to obtain plate specimens having a thickness of 1.0 mm. Solution heat treatment was performed at 480 ˚C for 5 min (Alloy A) or for 30 min (Alloy B) and water-quenched (WQ), artificial aging was performed at 120 ˚C for 48 h (T6-temper). Average grain size of the specimens after the heat treatment was 26.1 μm for Alloy A and 28.7 μm for Alloy B. Plate specimens for the tensile test with a gage length of 10 mm, width of 5 mm, fillet radius of 1.0 mm, and thickness of 1.0 mm were prepared by means of electrical discharge machining. In all the test specimens, both surfaces were polished by emery papers (#800 and #1200) and buffed with alumina pastes to obtain a mirror-finished surface. To reveal the hydrogen embrittlement sensitivity, slow strain rate testing (SSRT) was performed with a relative humidity of 90% (RH90) or 50 % (RH50) in a laboratory air atmosphere. For comparison, SSRT under an ultrahigh vacuum (UHV) atmosphere (10^{-6} Pa) was also performed. Initial strain rate of the SSRT was ranging from 1.7×10^{-6} s^{-1} to 2.5×10^{-2} s^{-1}.

Table 1 Chemical composition of Al-Zn-Mg base alloys (wt.%)

Alloy	Zn	Mg	Cu	Fe	Si	Ti	Al
A	5.6	2.5	<0.1	0.06	0.02	0.01	Bal.
B	5.6	2.5	2.0	0.06	0.02	0.01	Bal.

In the HMT [9,10], before the testing, a mirror-finished surface was covered with a collodion layer to prevent the reduction of Ag^+ to Ag by aluminum atoms. The collodion layer was then covered with a liquid nuclear emulsion (Ilford L-4, diluted with pure water) containing gelatin and silver bromide (AgBr) crystals using a wire loop method and dried for 15 min. The specimens were tensile-deformed in a laboratory air with a strain rate of $3.3 \times 10^{-3} s^{-1}$. After the fracture, the specimens were removed from the testing machine and dipped into formalin (37 mass% HCHO water solution) after the tensile test for 3 s to harden the gelatin layer; then, the specimens were immersed in a fixing solution (15 mass% $Na_2S_2O_3$ water solution) for 8 min to remove the remaining silver bromide particles that did not react with the hydrogen atoms. The arrangement of the silver particles was observed using a scanning electron microscope (SEM) equipped with an energy dispersive X-ray spectrometer (EDXS).

Apart from the SSRT, hydrogen gas evolution behavior during the tensile test was also examined as follows; the specimen was initially placed on the jig of the tensile testing apparatus equipped with a quadrupole mass spectrometer (QMS) installed in the UHV chamber as shown in Fig.1 originally developed by Kanno [11,12]. The tensile test of the specimens was carried out 24 h after maintaining the specimens in a UHV atmosphere in order to obtain a vacuum level of 7.0×10^{-7} Pa. In this study, a baking

operation for the UHV chamber was not performed in order to carry out the tensile test under the constant ambient temperature. The hydrogen gas evolution from the specimen was evaluated from the hydrogen ion current, where the mass number M/e=2 was selected. The QMS-UHV tensile test was carried out at strain rates of 3.3×10^{-3} s^{-1} and 2.5×10^{-2}s^{-1}.

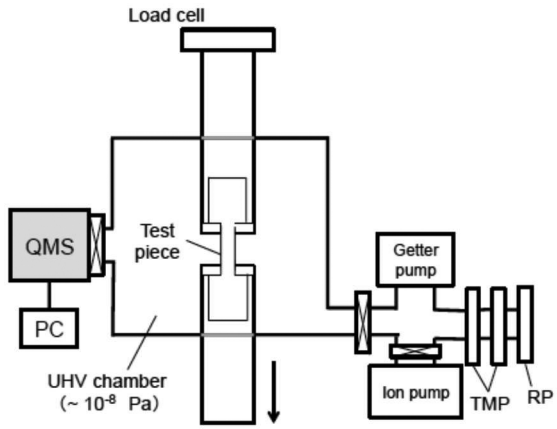

Fig.1 Schematic view of the testing machine with a mass spectrometer in the ultrahigh vacuum chamber.

Results and discussion

Figure 2 shows the fracture strain as a function of testing strain rate in the tensile test. The decrease of the fracture strain was obvious when the strain rate was lowered to the order of 10^{-6} s^{-1} in both specimens tested in air. The lowering of the fracture strain was more prominent when the relative humidity was high. In the UHV environment, no decrease of the fracture strain was observed even in the low strain rate testing. In addition, the specimens with Cu addition (Alloy B) indicated higher fracture strain than the specimen without Cu (Alloy A) in the SSRT tested in air. This indicates that the addition of copper can suppress the hydrogen embrittlemet, which corresponds well with the results indicated in the previous paper [8].

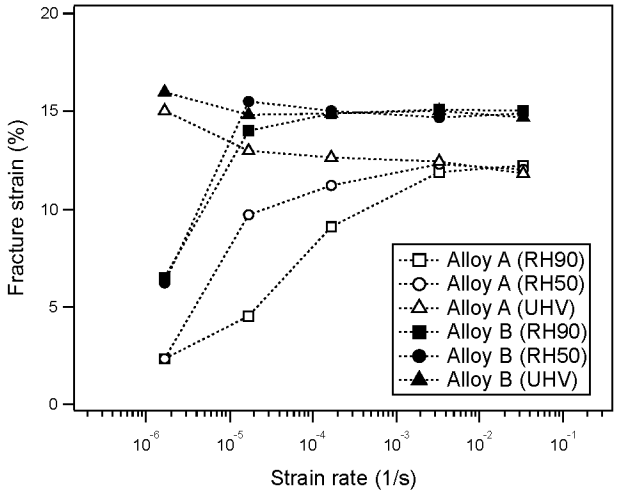

Fig.2 SSRT result of Al-Zn-Mg(-Cu) alloys.

Macroscopic fracture surface images after the tensile test under RH90 with a strain rate of 1.7×10^{-6} s^{-1} are shown in Fig.3. The Alloy A and B indicated both grain boundary (GB) fracture surfaces limited near the edge region (inside the frame) after the SSRT. When compared to the degree of the GB fracture, the area ratio of the GB fracture to entire fracture in the Alloy A was higher than Alloy B. The affected zone by atmospheric hydrogen was estimated to be about 500 μm in depth from the edge.

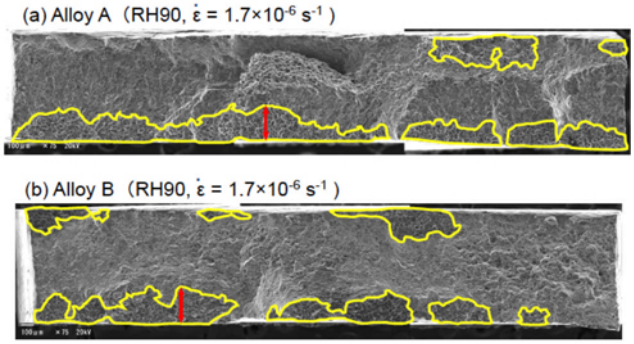

Fig. 3 Macroscopic fracture morphology of an Al-Zn-Mg alloy (a) and an Al-Zn-Mg-Cu alloy (b) after SSRT under a humid air atmosphere. Surrounding frame represents the area of grain boundary fracture.

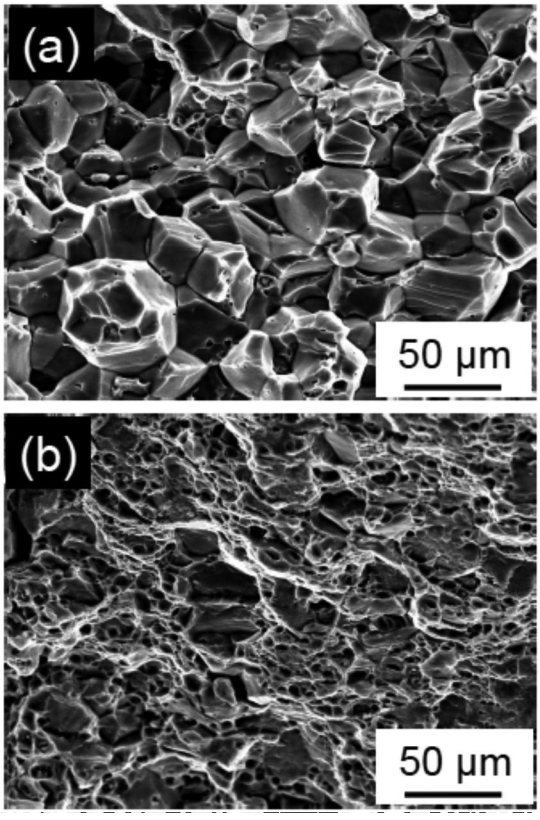

Fig.4 Magnified fracture surfaces corresponding to the edge surfaces of Fig.3. (a): Al-Zn-Mg alloy, (b): Al-Zn-Mg-Cu alloy.

Figure 4 shows the magnified images of the fracture surfaces in the similar region near the edge, corresponding to that shown in Fig. 3. The Alloy A (Fig.4(a)) fractured intergranularly and the Alloy B (Fig.4(b)) fractured almost transgranularly. It is thus apparent that the additional cupper would greatly suppress the intergranular fracture caused by atmospheric hydrogen.

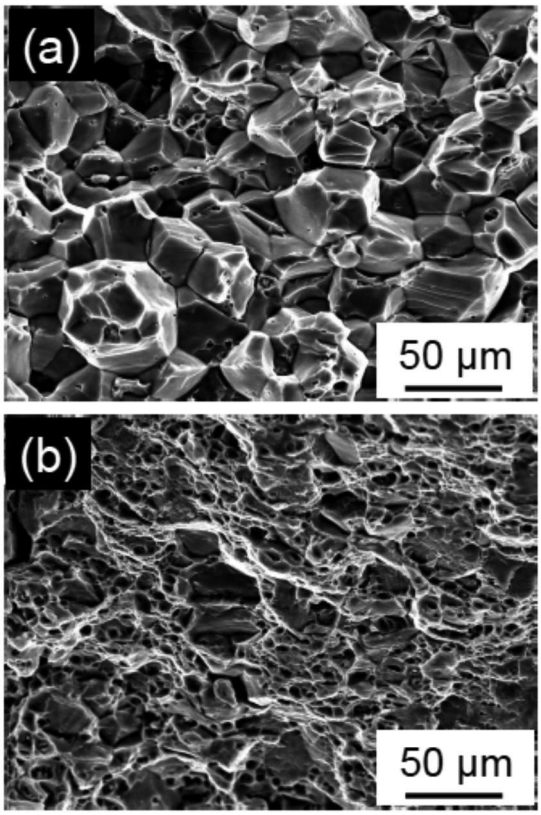

Fig.5 Deformed flat surfaces corresponding to the fracture surfaces of Fig.3. (a): Al-Zn-Mg alloy, (b): Al-Zn-Mg-Cu alloy.

Figure 5 shows the highly deformed surface morphology of Al-Zn-Mg alloy (a) and Al-Zn-Mg-Cu alloy (b) after SSRT under a humid air atmosphere corresponding to the specimens shown in Fig.3. The surface cracks were obvious particularly at GBs in the Al-Zn-Mg alloy, while that were observed at around inclusions as well as at GBs in the Al-Zn-Mg-Cu alloy. It is presumed that the difference of crack initiation sites would be related to resultant localized GB fractures.

In order to clarify the site of hydrogen emission in the deformed microstructure, HMT was performed for the specimens corresponding to the same condition as Fig.5. Figure 6 shows HMT images of the Alloy A, corresponding to the same testing condition as shown in Fig.6(a). White spherical particles representing Ag are arranged at grain boundaries (Fig.6(a)), slip lines (Fig.6(b)) and around second phase particles inside grains (Fig.6(c)). Both at GBs and slip lines, silver particles were not uniformly distributed. This implies that local hydrogen emission site is changeable according to the degree of local deformation state. EDX results revealed that the silver particles were detected from the periphery of AlFeSi base particles, not from the particle inside. This suggests that the interface of AlFeSi/Al becomes a rapid diffusion path of hydrogen atoms during tensile deformation.

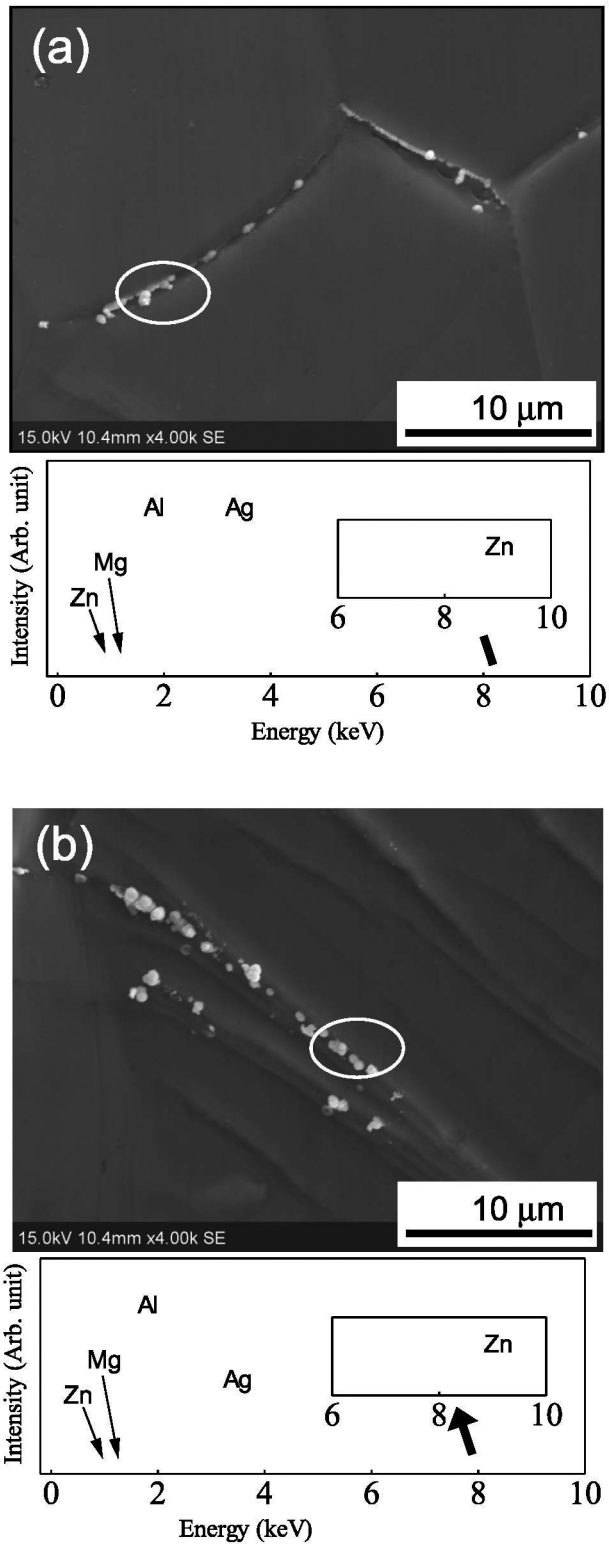

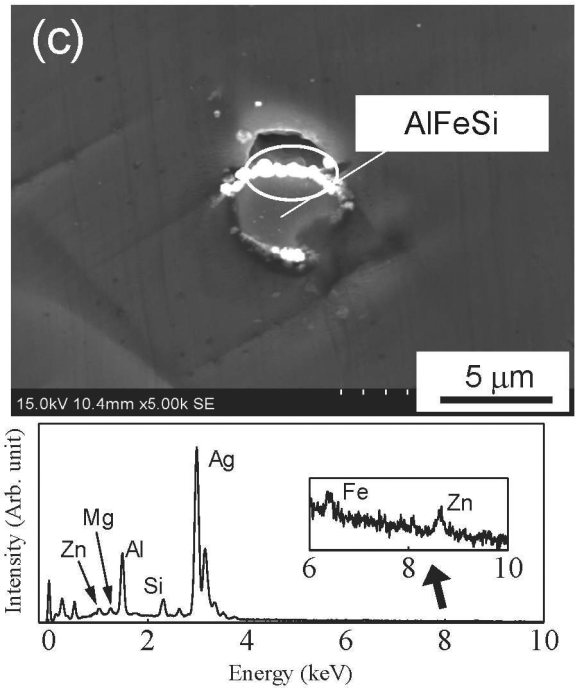

Fig.6 HMT images showing hydrogen emission site of deformed microstructure in the Al-Zn-Mg alloy corresponding to the same testing condition as shown in Fig.5(a). (a): GB, (b): slip line, (c): AlFeSi inclusion.

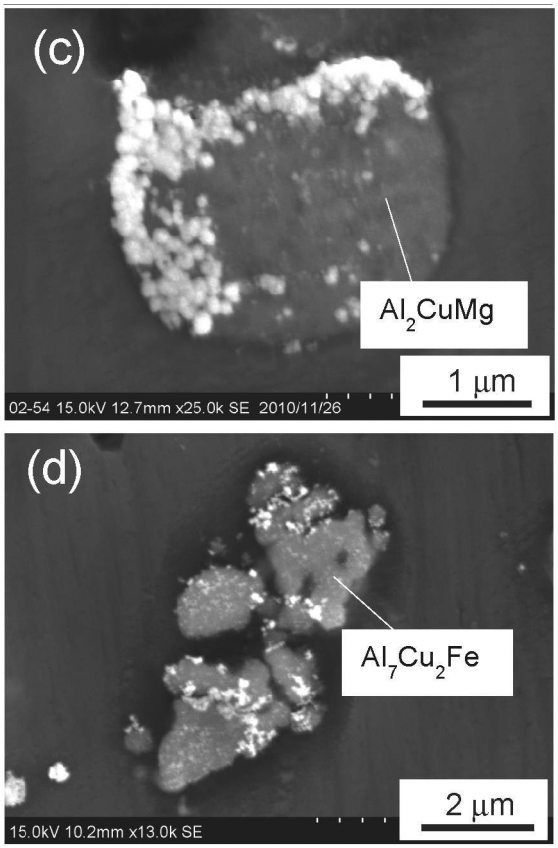

Fig.7 HMT images showing hydrogen emission site of deformed microstructures in the Al-Zn-Mg-Cu alloy corresponding to the same testing condition as shown in Fig.5(b). (a): GB, (b): Slip line, (c): AlCuMg inclusion, (d): AlCuFe inclusion.

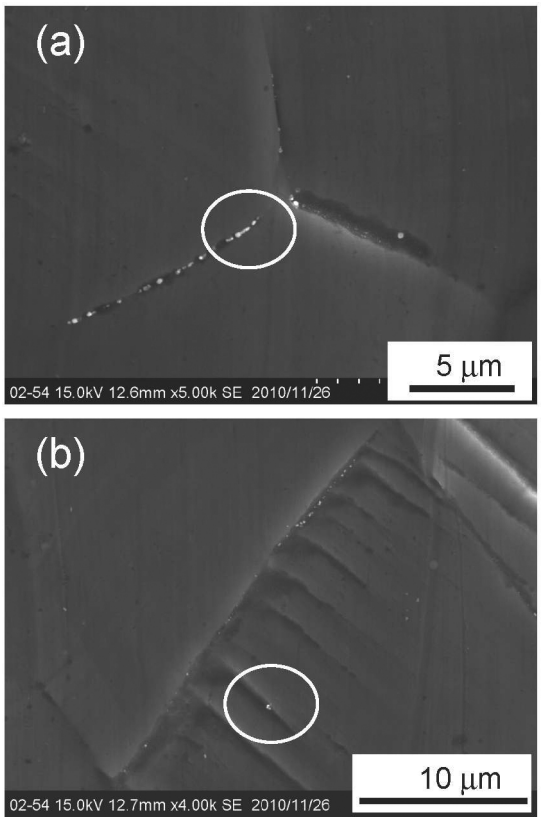

Figure 7 shows HMT images of the Alloy B, corresponding to the same condition as Fig.5(b). In a similar manner as Fig.6, silver particles were detected from grain boundaries (Fig.7(a)) and slip lines (Fig.7(b)). Silver particles were also detected from the constituent particles such as Al_7Cu_2Fe and Al_2CuMg existing in Al-Zn-Mg alloys with copper additions [8]. Silver particles were detected from almost all of the Cu-bearing particles. Additionally, in contrast to the Al-Zn-Mg alloy without copper as previously shown in Fig.6(c), silver particles were visible not only at the periphery of the particles but also at the particle inside in the Al-Zn-Mg-Cu alloy shown in Fig.7(c) and Fig.7(d). Hence, it is assumed that Cu-bearing particles would become the preferential diffusion site of hydrogen during deformation. By comparing the area density of Ag particles determined by using low magnification HMT images, it was shown that the Al-Zn-Mg-Cu alloy emitted high amount of hydrogen rather than the Al-Zn-Mg alloy, because of the distribution of high density of Cu-bearing particles.

Figure 8 shows the hydrogen gas evolution behavior during deformation and fracture determined by means of mass spectrometry under an ultrahigh vacuum atmosphere. Totally, the Al-Zn-Mg-Cu alloy evolved higher amount of hydrogen gas, rather than the Al-Zn-Mg alloy, which was good agreement with the HMT result as previously shown in Fig.7. The difference of

hydrogen gas evolution between these alloys might represent the difference of original hydrogen concentration.

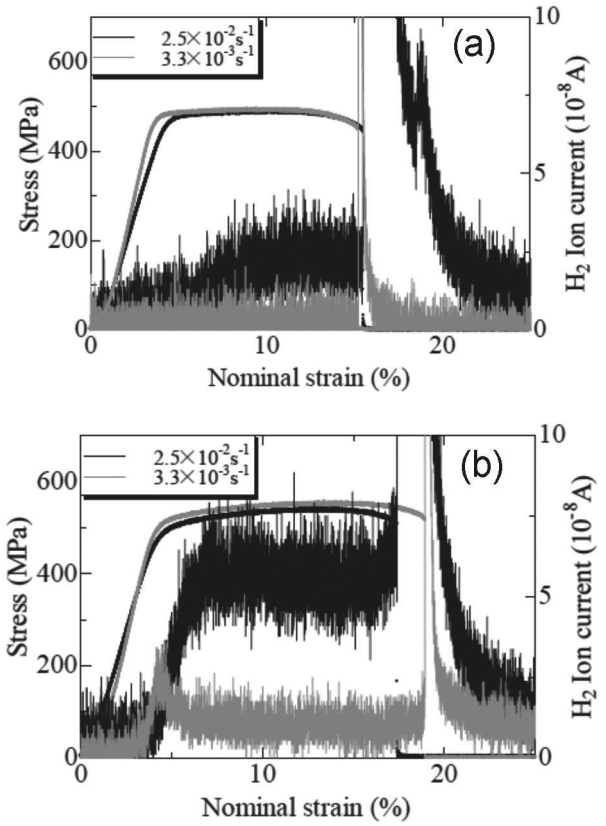

Fig. 8 Hydrogen gas evolution during the tensile test under ultrahigh vacuum atmosphere as a function of strain rate. (a): Al-Zn-Mg alloy, (b): Al-Zg-Mg-Cu alloy.

At near the yielding, hydrogen gas evolution peak was clearly identified particularly in the Al-Zn-Mg-Cu alloy. Since the timing of hydrogen evolution peak corresponds well to the yielding point, this hydrogen evolution behavior would be related to the interaction between Cu-bearing particles and dislocations. On possible source would be due to hydrogen transportation with an aid of mobile dislocation, as has been proposed [13]. Another possible sources could be related to stress-induced hydrogen diffusion around Cu-bearing particles. Since no evolution peaks of hydrogen were observed in the Al-Zn-Mg alloy at the yielding, it is probable that hydrogen atoms were trapped strongly inside Cu-bearing compounds prior to the test. Since the Al-Zn-Mg-Cu alloy shows low sensitivity against hydrogen embrittlement as previously shown in Fig.2 regardless of containing high amount of hydrogen, Cu-bearing compounds in the Al-Zn-Mg-Cu alloy would act as an effective trapping site of hydrogen by preventing the hydrogen accumulation at grain boundaries, leading to the low sensitivity for HE.

Summary

Hydrogen gas evolution during deformation and fracture of Al-Zn-Mg (-Cu) alloys was visualized by means of HMT and using the mass spectrometry in an UHV atmosphere. The results obtained are summarized as follows: (1) Al-Zn-Mg-Cu alloy evolved higher amounts of hydrogen in the stage of deformation and fracture rather than Al-Zn-Mg alloy. (2) HMT revealed that hydrogen was evolved at grain boundaries, slip lines, and around second phase particles during the tensile deformation. (3) Cu-bearing compounds trapped hydrogen effectively and would reduce the HE sensitivity of Al-Zn-Mg base alloys.

References

1. K. Horikawa, "Current research trends in aluminum alloys for a high-pressure hydrogen gas container" *Journal of Japan Institute of Light Metals*, 60 (2010), 542-547.

2. M. Andoh et al., "Effects of alloy compositions on hydrogen embrittlement of Al–Mg–Si based alloys" *Journal of Japan Institute of Light Metals*, 59 (2009), 81-86.

3. S. Osaki et al., "Effect of grain size on hydrogen embrittlement properties of 6061 aluminum alloys" *Journal of Japan Institute of Light Metals,* 58(2008), 139-145.

4. S. Osaki et al., "Hydrogen embrittlement properties of 7075 and 6061 aluminum alloys in humid air" *Journal of Japan Institute of Light Metals*, 56 (2006), 721-727.

5. M. Andoh, M. Senoo and M. Kanno, "Environmental embrittlement in air of Al–Zn–Mg–Cu alloys with Cr or Zr" *Journal of Japan Institute of Light Metals,* 57(2007), 19-24.

6. K. Horikawa, H. Yamada and H. Kobayashi, "Effect of strain rate on hydrogen gas evolution behavior during tensile deformation in 6061 and 7075 aluminum alloys" *Journal of Japan Institute of Light Metals,* 62(2012), 306-312.

7. H. Yamada, K. Horikawa and H. Kobayashi, "Hydrogen evolution behavior of tensile deformation process in 6061 and 7075 aluminum alloys" *Journal of Japan Institute of Light Metals,* 61(2011), 297-302.

8. G. A. Young Jr. and J. T. Scully, "The effects of test temperature, temper, and alloyed copper on the hydrogen-controlled crack growth rate on an Al-Zn-Mg-(Cu) alloy" *Metall. Mater. Trans. A,* 33 (2002), 101-115.

9. J. Ovejero-Garcia, "Hydrogen microprint technique in the study of hydrogen in steels" *Journal of Materials Science,* 20 (1985), 2623–2629.

10. K. Horikawa and K. Yoshida, "Visualization of hydrogen distribution in tensile-deformed Al-5%Mg alloy investigated by means of hydrogen microprint technique with EBSP analysis" *Materials Transactions,* 45 (2004), 315-318.

11. M. Kanno, H. Okada, and G. Itoh, "Equipment for detection of gasses emitted from metallic material during deformation" *Journal of Japan Inst. Metals*, 56 (1992), 1501–1502.

12. M. Kanno, H. Okada, and G. Itoh, "Detection of gasses evolved from metallic materials during deformation" *Journal of Japan Institute of Metals,* 59 (1995), 296–302.

13. J. K. Tien et al., "Hydrogen transport by dislocations" *Metall. Trans. A*, 7 (1976), 821–829.